

Entrance of a Bioartificial Capsule in a Pore

A. Diaz¹ and D. Barthès-Biesel²

Abstract: This paper deals with the numerical study of the flow of a bioartificial capsule in a long axisymmetric pore with a hyperbolic entrance. The capsule consists of an infinitely thin and hyperelastic membrane filled with a Newtonian liquid. The resolution of the problem is based on an integral formulation of Stokes equations along with a boundary element method. The model allows the study of the influence of various parameters such as the membrane rheology, the membrane elasticity, the viscosity ratio λ between the capsule fluid and the suspending fluid, the capsule shape and size.

Owing to the important number of parameters involved in the problem, the effect of viscosity ratio λ and of the membrane rheology are investigated separately in the regime of large deformations. Special attention is given to the influence of the capsule initial shape. Specifically, we have considered ellipsoidal capsules with aspect ratio $A/B=0.28$ which thus have the same sphericity index as red blood cells. It is found that the entrance of the capsule in the pore is very sensitive to the capsule shape and volume. The influence of viscosity ratio λ is important in cases where quasi-plugging of the pore is reached. The effect of capsule rheology is significant when the deformations are very large.

1 Introduction

A capsule consists of an internal liquid enclosed by a deformable membrane. Liquid filled artificial capsules have many industrial applications (pesticides, inks, toothpaste, cosmetics,...). In Biomedical Engineering, artificial capsules are used in drug delivery systems, artificial organs or cell therapy [Lim (1984); Kühtreiber, Lanza and Chick (1999)]. However, a liquid filled capsule is also an appropriate model of a simple cell like the red blood cell, which is a biconcave disk filled with a hemoglobin so-

lution and enclosed by an area incompressible thin lipid bilayer, lined with a protein network. A capsule will be a crude model for more complex cells with nuclei, such as eggs or white blood cells.

We consider capsules that are designed to be suspended in another liquid. The hydrodynamic forces due to the flow of the internal and external liquids lead to the deformation of the capsule, and sometimes to breakup. From the mechanical point of view, this constitutes a very interesting fundamental problem of fluid structure coupling. Here the fluid stresses are essentially viscous (the flow Reynolds number based on the particle dimensions is small) and the capsule membrane undergoes large displacements and deformations. The modeling of the response of a capsule to such hydrodynamic forces has two main applications. Firstly, it allows the prediction of the response of cells to physiological flows and possibly the diagnostic of pathological states. Secondly, since it is essential to control the deformation and breakup of artificial capsules, the model allows the optimization of the design of the particle and of its membrane.

Some models of capsule motion in unbounded shear flows are available. The case of an initially spherical capsule subjected to small deformations is amenable to analytical solutions [Barthès-Biesel and Rallison (1981); Barthès-Biesel and Sgaier (1985); Brunn (1983)]. For arbitrary initial geometry and large deformations, it is of course necessary to resort to a numerical model. Since the flows are governed by the Stokes equations, a popular method consists in using a boundary integral formulation, first applied successfully to liquid droplets [Rallison and Acrivos (1978)]. The advantage of this approach as compared to an Arbitrary Lagrangian-Eulerian [ALE, Le Tallec and Mouro (2001)] formulation is that it is not necessary to map the entire external fluid domain for the numerical solution of the problem but only its boundaries. Moreover, there is no need of an interface tracking method since the positions of the membrane points can be updated by a kinematic condition.

¹ UMR CNRS 6600, UTC, BP 20649, 60206 Compiègne, France

² Corresponding author:

tel : (33) 344 234 397

fax: (33) 344 204 813

e-mail: dbb@utc.fr

The boundary integral formulation of Stokes flows has been used for the study of large deformations of capsules in various configurations: equilibrium and break-up in an elongational flow of a capsule with a Mooney-Rivlin membrane [Li, Barthès-Biesel and Helmy (1988); Diaz, Pelekasis and Barthès-Biesel (2000)], with an area incompressible membrane [Pozrikidis (1990a)], or with a viscoelastic membrane [Diaz, Barthès-Biesel and Pelekasis (2001)]. The tri-dimensional deformation in a simple shear flow has been studied for capsules with a hyperelastic membrane [Pozrikidis (1995); Ramanujan and Pozrikidis (1998)] or an area incompressible membrane [Zhou and Pozrikidis (1995)]. The effect of the bending rigidity of the membrane on the capsule steady equilibrium was investigated recently [Kwak and Pozrikidis (2001); Pozrikidis (2001)].

Here we focus on a special situation where the capsule is forced to flow through a small pore. This corresponds to the microcirculation of blood in the small capillary vessels and to filtration of capsule or cell suspensions. Using lubrication theory, Secomb and Hsu (1996) designed an axisymmetric model for the flow of a red blood cell through a pore driven by a constant pressure drop. The cell membrane is area incompressible. Its viscosity is taken into account, but its bending rigidity is ignored. Moreover, on physiological arguments, it is assumed that the main viscous dissipation effects occur in the membrane rather than in the internal liquid.

A boundary integral model of the flow of a capsule in a pore allows accounting for the effects of the internal liquid viscosity, of the membrane elastic properties and of the geometry of the capsule. A hyperbolic [Leyrat-Maurin and Barthès-Biesel (1994)] or cylindrical pore with a hyperbolic entrance [Quéguiner and Barthès-Biesel (1997), *to be called I in the following*] has been considered. These studies have been conducted under the assumption of equal viscosity for the internal and external liquid phases. This restriction does not affect the steady state results but becomes important during the transient entrance or exit phases. In I, capsules with elastomer membranes or with area incompressible membranes were studied. However, owing to numerical limitations, only ellipsoids with an axis ratio of at most 0.67 could be considered. This aspect ratio is quite larger than the one (0.28) of an ellipsoid with the same surface to volume ratio as a red blood cell.

Here we present a boundary integral model of the entry

flow of a capsule into a long pore until a steady state is reached. Our model is more precise and powerful than Quéguiner and Barthès-Biesel's, in the sense that it allows the investigation of elongated axisymmetric shapes (with the same surface to volume ratio as a red blood cell) without the resort of smoothing or volume correction procedures. This is achieved by the introduction of some out-of-plane bending stiffness in the membrane constitutive behavior. In practice, a capsule membrane presents some bending rigidity due to the finite thickness of the constitutive elastic material (e.g. Green and Zerna 1964) or due to its molecular structure [Lipowski (1991)]. The model also accounts for different internal and external viscosity. Furthermore the entrance of the pore is less tapered than the one used in I. Special attention is given to the influence of the membrane constitutive law on the transient and steady behavior of the capsule. We consider two types of membrane constitutive equations based either on the Mooney-Rivlin law designed for elastomers or on Skalak law [Skalak, Tözeren, Zarda and Chien (1973)]. This last law was originally proposed for the area incompressible red blood cell membrane, but is otherwise quite general and can be applied to a whole class of membranes, area incompressible or not. Our results are then useful for artificial capsules subjected to large deformations.

The problem assumptions, equations and boundary integral formulation of Stokes equations are given in section 2. The boundary element method is detailed in section 3. The model predictions are presented and discussed in section 4 for a number of different cases where the respective roles of the capsule intrinsic physical parameters are investigated. In particular, burst of a capsule can be predicted.

2 Problem statement

2.1 Problem geometry

The problem geometry is similar to that studied in I. The pore is axisymmetric and consists of a long cylindrical tube of radius R_t and of a coaxial hyperbolic entrance. All lengths are scaled with R_t . A system of cylindrical coordinates (x, r, ϕ) is used where the x -axis is the tube axis and where the origin O is located on the tube entrance (Figure 1). The equations for a meridian of the pore (coordinates x^B, r^B, ϕ) are then:

$$\begin{aligned} (r^B)^2 - (x^B)^2 \tan^2 \alpha &= 1 & \text{for } x^B \leq 0, \\ (r^B)^2 &= 1 & \text{for } x^B > 0 \end{aligned} \quad (1)$$

where α is the angle between the axis of revolution and the asymptote of the hyperbolic pore.

2.2 Problem equations

The capsule reference geometry is a spheroid with axial semi-diameter A and radius B . It consists of a drop of a Newtonian incompressible liquid of viscosity $\lambda\mu$ enclosed by an infinitely thin impermeable membrane (M) with a surface shear elastic modulus G and a surface bending rigidity modulus D . The revolution axis of the particle is aligned with the tube axis so that the configuration is fully axisymmetric (Figure 1). The pore is filled with a Newtonian incompressible liquid of viscosity μ which flows with a constant flow rate Q . The tube is supposed to be sufficiently long to allow the capsule to reach a steady motion in the cylindrical part.

2.2.1 Membrane mechanics

Under the hypothesis of infinitesimal thickness, the 3D stresses in the deformed membrane are replaced by tensions (forces per unit length) and bending moments (moments per unit length). Because of the specific geometry of the problem, the deformation of the membrane is purely axisymmetric with no torsion. Consequently the material points remain on the same membrane meridian during this process. In the reference configuration, the points of the membrane are labeled by their co-ordinates (X, R, ϕ) in the system of cylindrical co-ordinates defined in section 2.1, or by the arc length S along a meridian curve ($S=0$ at the upstream pole). In the deformed configuration, the surface points co-ordinates are $(x(S, t), r(S, t), \phi)$ with arc length $s(S, t)$ ($s(0, t)=0$). The principal directions of stress and strain are along the meridian (index s) and azimuth (index ϕ). The membrane deformation may be defined in terms of the principal extension ratios λ_s and λ_ϕ :

$$\lambda_s = \frac{ds}{dS}, \quad \lambda_\phi = \frac{r}{R}. \quad (2)$$

The associated principal curvatures κ_s and κ_ϕ are :

$$\kappa_s = -\frac{dt}{ds} \cdot \mathbf{n}, \quad \kappa_\phi = \frac{n_r}{r}, \quad (3)$$

where \mathbf{t} is the unit tangent vector oriented in the direction of increasing s and \mathbf{n} the outer unit normal vector to the capsule.

The membrane is supposed to be isotropic in its plane, of the hyperelastic type and to deform at constant temperature. Two membrane constitutive laws are considered in this work: a Mooney-Rivlin law and a Skalak law [Skalak, Tözeren, Zarda and Chien (1973)]. For each law, the principal meridional tension is given. The azimuthal principal tension is obtained by interchanging the subscripts s and ϕ .

In the case of a Mooney-Rivlin law, the membrane corresponds to the infinitely thin limit of a tri-dimensional hyperelastic and incompressible rubber-like material. The membrane initial thickness is uniform. The simplest neo-Hookean form (NH) of this law is given by Green & Adkins (1970):

$$T_s = \frac{G}{\lambda_s \lambda_\phi} \left(\lambda_s^2 - \frac{1}{(\lambda_s \lambda_\phi)^2} \right), \quad (4)$$

where G is a surface shear elastic modulus. According to the assumption of 3D incompressibility, the thickness decreases when the membrane surface area increases. Such a law, would then be appropriate for an homogeneous gelatin membrane which is almost 3D incompressible.

For a material obeying the Skalak law (noted SK), the tension and extension ratio are related by :

$$T_2 = \frac{G}{\lambda_s \lambda_\phi} [\lambda_s^2 (\lambda_s^2 - 1) + C (\lambda_s \lambda_\phi)^2 (\lambda_s^2 \lambda_\phi^2 - 1)]. \quad (5)$$

The first term of the right hand side of equation (5) corresponds to the contribution of shear deformations (with associated surface modulus G). The second term arises from surface dilatation (with associated surface modulus CG). Originally, this law was designed to model the red blood cell membrane. Such a membrane is almost area-incompressible but easy to shear. It is then usual to study the prediction of this law in the limit $C \gg 1$. However, (5) is very general and may be also applied to surface compressible membranes by taking $O(1)$ values for C . This may be particularly useful for polymerized interfaces or for gelatin membranes reinforced by a polymer network [Levy and Edwards-Levy (1996)], which may not be well represented by a neo-Hookean law. Barthès-Biesel, Diaz

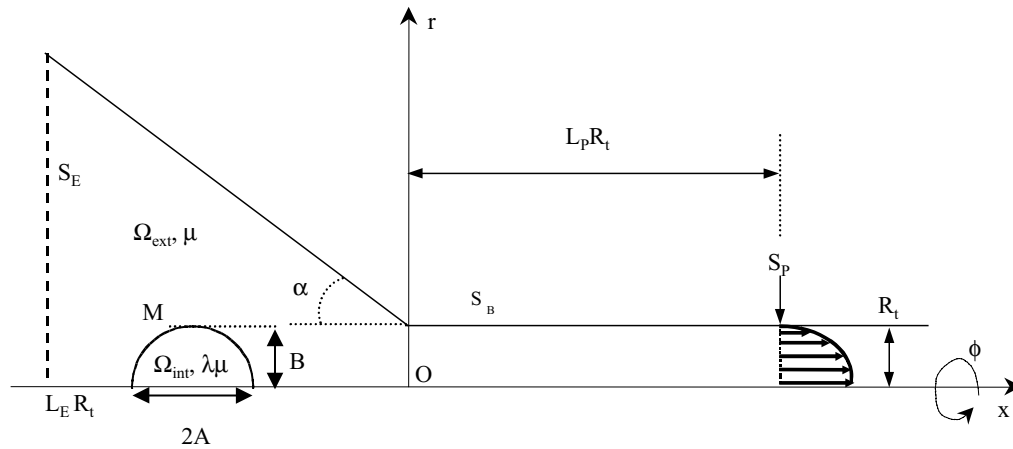


Figure 1 : Schematic description of the problem

and Dhenin (2002) show that for $C=1$, a NH membrane and a SK membrane have the same small deformation behavior (i.e., same shear, Young and area dilatation moduli). However, for large deformations, the NH membrane is strain softening, whereas the SK membrane is strain hardening for all values of C ($C > 0$).

In the present problem, the capsule membrane may be subjected to compressive tensions. It is thus useful to take into account the bending rigidity of the membrane. As a first approximation, the bending moments are, M_s, M_ϕ expressed as linear combinations of the change in principal curvatures [Zarda, Chien and Skalak (1977)]:

$$\begin{aligned} M_s &= \frac{D}{\lambda_\phi} (\lambda_s \kappa_s - \kappa_s^0 + \nu (\lambda_\phi \kappa_\phi - \kappa_\phi^0)), \\ M_\phi &= \frac{D}{\lambda_s} (\lambda_\phi \kappa_\phi - \kappa_\phi^0 + \nu (\lambda_s \kappa_s - \kappa_s^0)) \end{aligned} \quad (6)$$

where κ_s^0 and κ_ϕ^0 represent the principal curvatures of the membrane in the reference state. The parameter ν is equivalent to a two-dimensional Poisson ratio, it is equal to $C/(1+C)$ for a SK membrane and to $1/2$ for a NH membrane. The coefficient D is the surface bending modulus. In the range of small deformations and small variations of curvature, the law (6) is analogous to the relation between moments and curvatures that would be obtained for a thin sheet of a Hookean material. This law is thus very simple and does not depend on the structure of the membrane. The lack of information on the bending properties of natural cells or of artificial capsules membranes excludes however the consideration of more complicated laws.

The shell equilibrium equations provide a relation between the elastic tensions, the bending moments and the load per unit of deformed area $-\mathbf{q}$:

$$\begin{aligned} \mathbf{q} \cdot \mathbf{t} &= \frac{dT_s}{ds} + \frac{1}{r} \frac{dr}{ds} (T_s - T_\phi) - \kappa_s \left(\frac{1}{r} \frac{dr}{ds} M_\phi - \frac{1}{r} \frac{d}{ds} (r M_s) \right) \\ \mathbf{q} \cdot \mathbf{n} &= -\kappa_s T_s - \kappa_\phi T_\phi - \frac{1}{r} \frac{d}{ds} \left[\left(\frac{dr}{ds} M_\phi - \frac{d}{ds} (r M_s) \right) \right]. \end{aligned} \quad (7)$$

2.2.2 Equations of motion for the fluids

It has been shown theoretically for a pore with the most severe opening ($\alpha = 90^\circ$) that, in absence of particle, a Poiseuille velocity profile is observed for $x = 1/2$ [Dagan, Weinbaum and Pfeffer (1982)]. It was observed in I, that in presence of a capsule, a Poiseuille profile is recovered within 1% at one pore radius upstream and downstream from the capsule tips. Furthermore, when the pore is sufficiently long to allow the capsule to reach a steady state, the entrance phase is independent from the exit phase. We shall thus focus on the entrance of a capsule in an infinitely long pore under constant flow rate. The external fluid domain Ω_{ext} is accordingly delimited by the pore walls S_B , an entrance section S_E , an exit section S_P located at $x=L_P$ and the capsule membrane M . The domain occupied by the internal fluid is denoted Ω_{int} and is delimited by M . The meridians of the boundaries S_B and M are respectively denoted C_B and C_M . The radius of S_P is denoted C_P .

Non dimensional variables are used throughout: lengths are scaled with R_t , velocities with $Q/\pi R_t^2$, viscous

stresses and pressure by $\mu Q/\pi R_t^3$, elastic tensions by G and bending moments by GR_t . The dimensionless parameters governing the capsule dynamics are accordingly:

- the capsule initial aspect ratio: A/B ,
- the ratio between the radius of the sphere with the same volume as the capsule and the pore radius: $R_{eq}=(AB^2)^{1/3}/R_t$,
- the ratio between internal and external fluid viscosity: λ ,
- the capillary number: $\varepsilon = \frac{\mu Q}{\pi R_t^2 G}$,
- the bending ratio: $\delta=D/GR_t^2$

The Reynolds number based on the capsule dimension is supposed to be very small. Consequently, the motion of the outer fluid is described by the Stokes equations :

$$\begin{aligned} \nabla \cdot \mathbf{v}^{\text{ext}}(\mathbf{x}) &= \mathbf{0} \\ \nabla \cdot \boldsymbol{\sigma}^{\text{ext}}(\mathbf{x}) &= \mathbf{0} \end{aligned} \quad \text{for } \mathbf{x} \in \Omega_{\text{ext}} \quad (8)$$

where \mathbf{v}^{ext} is the velocity field and $\boldsymbol{\sigma}^{\text{ext}}$ the stress tensor given by Newton's law. The same equations obviously apply for the internal flow (\mathbf{v}^{int} , $\boldsymbol{\sigma}^{\text{int}}$). The boundary conditions associated to the Stokes equations are :

a) no slip and membrane impermeability:

$$\mathbf{v}^{\text{ext}}(\mathbf{x}) = \mathbf{v}^{\text{int}}(\mathbf{x}) = \mathbf{v}^M(\mathbf{x}) \quad \text{for } \mathbf{x} \in M, \quad (9)$$

$$\mathbf{v}^M(\mathbf{x}) = \partial \mathbf{x} / \partial t \quad \text{for } \mathbf{x} \in M, \quad (10)$$

where \mathbf{v}^M is the membrane velocity.

b) dynamic membrane equilibrium:

$$\varepsilon(\boldsymbol{\sigma}^{\text{ext}} - \boldsymbol{\sigma}^{\text{int}}) \cdot \mathbf{n} = -\mathbf{q} \quad \text{for } \mathbf{x} \in M, \quad (11)$$

c) no-slip and impermeability on the tube wall S_B :

$$\mathbf{v}^{\text{ext}}(\mathbf{x}) = \mathbf{0} \quad \text{for } \mathbf{x} \in S_B, \quad (12)$$

d) the entrance section S_E is located in the reservoir at a distance L_E that is far from the tube entrance (here $L_E=30$). As shown in I, the pressure on S_E is uniform within and set to zero.

$$P^{\text{ext}} = 0 \quad \text{for } \mathbf{x} \in S_E. \quad (13)$$

e) the section S_P is located at a position $x=L_P$ (here $L_P=15$) which is far enough downstream in the tube for Poiseuille flow to prevail :

$$\mathbf{v}^{\text{ext}}(\mathbf{x}) = 2(1-r^2)\mathbf{e}_x \quad \text{at } x = L_P, \quad (14)$$

The solution of the equations of motion with boundary conditions (9) to (14), leads to the values of the pressure P^{ext} in section S_E .

$$P^{\text{ext}} = P_{np}^P + \Delta P \quad \text{at } x = L_P, \quad (15)$$

where P_{np}^P is the pressure in absence of particle and ΔP the unknown additional pressure drop that varies as the capsule enters the pore.

2.2.3 Boundary integral formulation

A boundary integral formulation is used for the fluid problem. This method is particularly well adapted to free surface flows because it allows to relate the membrane velocity \mathbf{v}^M at a point \mathbf{x} of the interface M to the velocity and force distributions on the boundaries $S_B \cup S_P \cup S_E \cup M$. Boundary integral formulations of Stokes equations have been used to compute the motion and deformation of different particles suspended in a flowing liquid: bubbles [Youngren and Acrivos (1976)], drops [Rallison and Acrivos (1978), Pozrikidis (1990b), Stone and Leal (1989), Martinez and Udell (1990), Couillette and Pozrikidis (1998)], capsules (Li, Barthès-Biesel and Helmy (1988); Leyrat-Maurin and Barthès-Biesel (1994); Quéguiner and Barthès-Biesel (1997); Pozrikidis (1995); Zhou and Pozrikidis (1995); Ramanujan and Pozrikidis (1998); Diaz, Pelekasis and Barthès-Biesel (2000); Kwak and Pozrikidis (2001); Pozrikidis (2001)].

In the present case, the velocity of a point \mathbf{x} located on $S_B \cup S_P \cup S_E \cup M$ is given by:

$\beta v_j(\mathbf{x}) =$

$$\frac{1}{8\pi\epsilon} \int_M J_{ji}(\mathbf{x}, \mathbf{y}) q_i(\mathbf{y}) dA(\mathbf{y}) + (\lambda - 1) \int_M v_i(\mathbf{y}) K_{ijk}(\mathbf{x}, \mathbf{y}) n_k(\mathbf{y}) dA(\mathbf{y}) \quad (16)$$

$$\frac{1}{8\pi} \int_{S_B \cup S_p \cup S_E} J_{ji}(\mathbf{x}, \mathbf{y}) f_i(\mathbf{y}) dA(\mathbf{y}) - \int_{S_p \cup S_E} v_i(\mathbf{y}) K_{ijk}(\mathbf{x}, \mathbf{y}) n_k(\mathbf{y}) dA(\mathbf{y})$$

Boundary conditions (9), (11) and (12) have been taken into account. The force \mathbf{f} is the force exerted by the boundary on the external fluid and $dA(\mathbf{y})$ a surface element. The value of the parameter β depends on position \mathbf{x} :

$$\begin{aligned} \beta &= \frac{1 + \lambda}{2} \text{ for } \mathbf{x} \in M, \\ \beta &= 0 \text{ for } \mathbf{x} \in S_B, \\ \beta &= \frac{1}{2} \text{ for } \mathbf{x} \in S_p \cup S_E. \end{aligned} \quad (17)$$

The tensors \mathbf{J} and \mathbf{K} are the Green functions for an unbounded Stokes flow and correspond respectively to the single and double-layer potentials. They are known functions of position:

$$\begin{aligned} J_{ji}(\mathbf{x}, \mathbf{y}) &= \frac{\delta_{ji}}{|\mathbf{x} - \mathbf{y}|} + \frac{(\mathbf{x} - \mathbf{y})_j (\mathbf{x} - \mathbf{y})_i}{|\mathbf{x} - \mathbf{y}|^3}, \\ K_{ijk}(\mathbf{x}, \mathbf{y}) &= -\frac{3}{4\pi} \frac{(\mathbf{x} - \mathbf{y})_i (\mathbf{x} - \mathbf{y})_j (\mathbf{x} - \mathbf{y})_k}{|\mathbf{x} - \mathbf{y}|^5}. \end{aligned} \quad (18)$$

On S_E , \mathbf{J} and \mathbf{K} are respectively at most $O(1/L_E)$ and $O(1/L_E^2)$ while dA is $O(L_E^2)$. The average velocity on S_E is $O(1/L_E^2)$, consequently the contribution of S_E to the 4th integral of the right hand side of (16) is negligible.

When $\mathbf{y} = \mathbf{x}$, \mathbf{J} and \mathbf{K} are singular and the integrals of (17) become improper. The single-layer potential may be

shown to converge (because of the order of the singularity) and the double-layer must be taken in the principal value sense. The latter may be regularized [Pozrikidis (1990b)]. Since the problem considered in the present work is axisymmetric, the integration in the azimuthal direction may be performed analytically and the surface integrals of (17) reduce to curvilinear integrals taken along the corresponding meridian curves and along the radius of S_p [Pozrikidis (1992)].

3 Numerical procedure

The numerical method used here is similar to that used by Diaz, Pelekasis and Barthès-Biesel (2000). It consists in following the transient response of the initially undeformed capsule to the start of the flow. At time $t=0$, the undeformed capsule is placed far downstream from S_E and far upstream from the tube entrance. The algorithm consists in following its motion and deformation as it flows into the pore until a steady state is reached. The adopted approach is Lagrangian: at each time step the position of the membrane material points is known. Consequently \mathbf{q} can be easily obtained from (2) to (7). The unknowns of the problem are then the force \mathbf{f}^B on S_B , the perturbed pressure $P_{np}^P + \Delta P$ at $x=L_P$ and the velocity of the capsule membrane \mathbf{v}^M . The unknowns are determined from the solution of the axisymmetric and ϕ -integrated form of (16) written for $\mathbf{x} \in C_M, C_B, C_p$. Finally, the kinematic condition (10) allows to obtain the new position of the material points and the next deformed profile by means of a simple time integration. This method enables an

The axisymmetric and ϕ -integrated form of integral equation (16) is treated by means of a boundary element method. The meridians C_M, C_B and C_p are partitioned in respectively N_M, N_B and N_p two-nodes elements E_e delimited by the nodes \mathbf{y}^e and \mathbf{y}^{e+1} . The N_M+1 nodal points are unevenly spaced along C_M with a higher density in the regions of large curvatures. The partition of C_B and C_p are similar to that used in I.

The geometry of each curvilinear boundary element E_e of the meridian C_M is approximated using the following parametric relation:

$$\mathbf{y}(\zeta) = \begin{vmatrix} y_x(\zeta) \\ y_r(\zeta) \end{vmatrix} = \sum_{j=0}^{N_M+2} \begin{vmatrix} \Psi_x^j \\ \Psi_r^j \end{vmatrix} BS^j(\zeta). \quad (19)$$

The parameter ζ is such that $\mathbf{y}^e = \mathbf{y}(\zeta^e)$ and $\mathbf{y}^{e+1} = \mathbf{y}(\zeta^{e+1})$. The shape functions BS^j ($j = 0, \dots, N_M + 2$) are cubic B-splines. Cubic splines are piece-wise polynomials of degree 3 that guarantee the continuity at the nodes of the interpolant \mathbf{y} and of its first and second derivatives (DeBoor 1978). For a given degree of interpolation, B-splines are nonzero over the smallest possible number of consecutive elements. In the present case BS^j is non zero over the interval $[\zeta^{j-2}; \zeta^{j+2}]$. The sets $\{\psi_x^j\}, \{\psi_r^j\}$ ($j = 0, \dots, N_M + 2$) are the spline interpolation coefficients. The computation of the coefficients $\{\psi_x^j\}$ (respectively $\{\psi_r^j\}$) from the abscissa of the nodes y_x^i (respectively y_r^i) necessitates the solution of a system of $N_M + 3$ equations with $N_M + 3$ unknowns. The $N_M + 1$ first equations are given by :

$$y_x(\zeta^e) = \sum_{j=0}^{N_M+2} \psi_x^j BS^j(\zeta^e), \quad e = 1, \dots, N_M + 1. \quad (20)$$

Two additional equations are provided by symmetry conditions at the extremities of the meridian C_M . The assumptions of a closed, regular and axisymmetric surface lead to:

$$\frac{\partial y_x}{\partial \zeta} = 0 \text{ for } \zeta = \zeta_{\max} \text{ and } \zeta = 0. \quad (21)$$

For y_r , a relation similar to (20) is written and the appropriate symmetry conditions are :

$$\frac{\partial^2 y_r}{\partial \zeta^2} = 0 \text{ in } \zeta = \zeta_{\max} \text{ and } \zeta = 0. \quad (22)$$

The unit tangent vector and the second order surface properties are readily computed from the derivation of (19). Cubic B-splines are respectively $O(\Delta\zeta^4)$, $O(\Delta\zeta^3)$ and $O(\Delta\zeta^2)$ accurate in interpolating a smooth function, its first and second derivatives (where $\Delta\zeta$ denotes a typical variation of ζ over one element). Cubic B-splines interpolation allows a precise computation of the tangent vector and principal curvatures which is essential for applications to membrane mechanics problems, where second order surface properties are needed.

Although the pore geometry is very simple, the same B-spline interpolation scheme is chosen for C_B for the sake

of consistency. Moreover, this method makes it simple to tackle more complicated pore shapes. The following procedure is used to generate two end conditions: at each extremity of C_B , the value of $\partial y / \partial \zeta^B$ is evaluated numerically by constructing a cubic lagrangian interpolant of y over the four first (or last) nodes. This interpolation is not expected to affect much the overall accuracy of the method since the lagrangian interpolation is of the same order of accuracy as the cubic B-spline interpolation. The corresponding boundary condition is then obtained by setting $\partial y / \partial \zeta^B$ equal to the interpolated value.

Since the geometry of the membrane M and of the tube S_B is known at any time step, the above spline interpolation coefficients are known. Cubic B-splines are also used to interpolate the unknowns \mathbf{v}^M and \mathbf{f}^B :

$$\mathbf{v}^M(\zeta) = \begin{vmatrix} v_x^M(\zeta) \\ v_r^M(\zeta) \end{vmatrix} = \sum_{j=0}^{N_M+2} \begin{vmatrix} \psi_x^j \\ \psi_r^j \end{vmatrix} BS^j(\zeta), \quad (23)$$

and,

$$\mathbf{f}^B(\zeta^B) = \begin{vmatrix} f_x^B(\zeta^B) \\ f_r^B(\zeta^B) \end{vmatrix} = \sum_{j=0}^{N_B+2} \begin{vmatrix} \phi_x^j \\ \phi_r^j \end{vmatrix} BS^j(\zeta^B). \quad (24)$$

The associated symmetry conditions for the membrane velocity \mathbf{v}^M are:

$$\frac{\partial \mathbf{v}_x^M}{\partial \zeta} = 0 \text{ for } \zeta = \zeta_{\max} \text{ and } \zeta = 0, \quad (25)$$

$$\frac{\partial^2 \mathbf{v}_r^M}{\partial \zeta^2} = 0 \text{ for } \zeta = \zeta_{\max} \text{ and } \zeta = 0. \quad (26)$$

At the extremity of C_B corresponding to the entrance of the pore ($\zeta^B = 0$), the axial and radial components of \mathbf{f}^B are nearly zero and vary weakly with ζ^B . Appropriate end conditions are thus :

$$\frac{\partial f_x^B}{\partial \zeta^B} = 0 \text{ and } \frac{\partial^2 f_r^B}{\partial \zeta^{B2}} = 0 \text{ for } \zeta^B = 0. \quad (27)$$

The other extremity of C_B corresponds to the intersection with the meridian on which a Poiseuille flow is recovered. The conditions for \mathbf{f}^B are thus:

$$f_x^B(\zeta^B) = -4 \text{ and } \frac{\partial^2 f_r^B}{\partial \zeta^{B2}} = 0 \text{ for } \zeta^B = \zeta_{\max}^B. \quad (28)$$

The B-spline interpolations of the geometry of C_M and C_B are used in the axisymmetric and ϕ -integrated form

of equation (16). The integrals over C_M , C_B and C_P are decomposed into a sum of elementary integrals taken over each boundary element. Regular integrals are computed by means of regular 5-point Gauss quadrature. For singular integrals, the singularity is logarithmic and integration is performed by means of a 12-point logarithmic quadrature. This ensures that the numerical error is due to the interpolation procedure rather than to the numerical integration (Stroud & Secrest 1966). A set of $2(N_M+N_B+3)$ unknowns arises from the incorporation of the B-spline interpolation ((23) and (24)) and conditions ((25) to (28)) into the ϕ -integrated form of (16). Requiring this equation to be satisfied at each of the N_M nodes of C_M , the N_B nodes of C_B and at the point $x=L_P$, a matrix equation is obtained:

$$\underbrace{\begin{pmatrix} \mathbf{L}_{11} & \mathbf{L}_{12} & \mathbf{L}_{13} \\ \mathbf{L}_{21} & \mathbf{L}_{22} & \mathbf{L}_{23} \\ \mathbf{L}_{31} & \mathbf{L}_{32} & \mathbf{L}_{33} \end{pmatrix}}_{\mathbf{L}} \begin{pmatrix} \varpi_x^0 \\ \varpi_r^0 \\ \vdots \\ \vdots \\ \varpi_x^{N_M+2} \\ \varpi_r^{N_M+2} \\ \varphi_x^0 \\ \varphi_r^0 \\ \vdots \\ \vdots \\ \varphi_x^{N_B+2} \\ \varphi_r^{N_B+2} \\ P_{np}^P + \Delta P \end{pmatrix} = \underbrace{\begin{pmatrix} \mathbf{H}_1 \\ \mathbf{H}_2 \\ \mathbf{H}_3 \end{pmatrix}}_{\mathbf{H}}. \quad (29)$$

The matrix \mathbf{L} is divided into nine blocks. The lines 1, 2 and 3 respectively correspond to the case where the collocation point is on C_M , on C_B or at $x=L_P$ on C_P . The columns 1, 2, 3 respectively correspond to the contributions of the double-layer potential for the velocity \mathbf{v}^M , the single-layer potential for the traction at the wall \mathbf{f}^B and the single-layer potential for the pressure $P_{np}^P + \Delta P$. The right hand side \mathbf{H} contains the contributions of the single-layer potential for the load $-\mathbf{q}$ and the force on C_P as well as the contributions of the double-layer potential for the Poiseuille velocity given by equation (14)

At each time step, the position of the membrane meridional nodes is known and the coefficients of the matrix \mathbf{L} , which are functions of the geometry of the boundaries, are computed. A standard LU decomposition method is used for the solution of (29). The shape of the capsule

is then updated by means of equation (10) which is time integrated with an explicit first order Euler-scheme.

4 Results

The capsule behavior depends on many different parameters. We have focussed our attention on the effect of:

- the viscosity ratio λ on the transient entrance of the capsule into the pore;
- a neo-Hookean (NH) or a Skalak (SK) constitutive equation for the membrane;
- the volume for spherical capsules ($R_{eq}=0.8; 0.9$ or 1.1);
- the initial geometry for spheres or ellipsoids. Specifically, we have considered ellipsoidal capsules with aspect ratio $A/B=0.28$, which thus have the same sphericity index as red blood cells.

The model computes the additional pressure drop ΔP , the position x_g and velocity v_g of the capsule center of mass as functions of time or of position along the tube axis. Furthermore, at each time step, the capsule deformed profile is determined, as well as the distribution of elastic tensions and deformations in the membrane.

Unless specified otherwise, the tube opening corresponds to $\alpha = 78.5^\circ$. It is close to that of filtration micropores [Reid, Barnes, Lock and Dormandy (1976)]. The Stokes model is adequate for describing the flow through such micropores. In cell transit analyzer (CTA) experiments for example, micropores are usually $5 \mu\text{m}$ in diameter and $15 \mu\text{m}$ in length. The pressure across the filtration membrane varies between 100 and 1000 Pa and the external fluid is a buffer or a Dextran solution [Fisher, Wenby and Meiselman (1992)]. The Reynolds number of the flow in the pore is therefore much smaller than 1.

The starting position of the capsule center of mass is $x_g=-4$. This was found to be far enough upstream of the pore entrance for the results to be independent of the particle initial position. For standard cases, the number of points on the pore wall and the exit section are $N_B=120$ and $N_P=30$.

4.1 Effect of bending rigidity

The entrance of any capsule in a long cylindrical pore consists of successive phases of aspiration, compression and then relaxation to steady state. For a sphere

($A=B=0.8$, $\epsilon=0.12$, $\lambda=1$), the compression phase happens for $x_g > 1$. The back of the capsule membrane is then subjected to in-plane compression in both principal directions s and ϕ . If the membrane out-of-plane bending rigidity is zero or too small, the membrane wrinkles or buckles locally (Figure 2) and it can be physically unstable. A small amount of bending stiffness can be introduced to prevent this phenomenon and stabilize the membrane. The objective of the present work is to study the deformations of the capsule in absence of buckling but not to investigate systematically of the effect of the bending ratio δ . Correspondingly, we have selected the smallest value of δ that leads to bending moments large enough to sustain in-plane compressive tensions. This

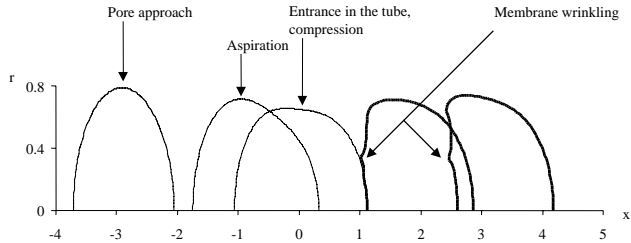


Figure 2 : Profiles of an initially spherical capsule devoid of bending stiffness during entrance in the pore ($A=B=0.8$, $\epsilon=0.12$, $\lambda=1$, NH membrane).

minimal compensatory stiffness depends on many parameters such as the geometry of the entrance of the pore, the value of the capillary number, the membrane law and the capsule initial shape. Several values of δ ($\delta = 10^{-9}$; 10^{-5} ; 10^{-4} ; 10^{-3}) were tested in the case of an initially spherical capsule ($A=B=0.8$) with a NH membrane and large deformations ($\epsilon = 0.12$). For values preventing local buckling, the effect of δ on the pressure drop is weak, as shown on Figure 3. Consequently, for each case, the smallest value of δ (10^{-5} for this case) which prevents buckling was selected.

4.2 Validation of results

There is no available analytical solution for the problem presented in this paper. However, when the capsule has reached a steady state, it behaves like a solid particle. The inner fluid is at rest, and the velocity of any membrane point is equal to that of the capsule center of mass. Consequently, the steady state does not depend on λ and the values of $|v_x^M - v_g|$ and $|v_r^M|$ should go to zero. Since

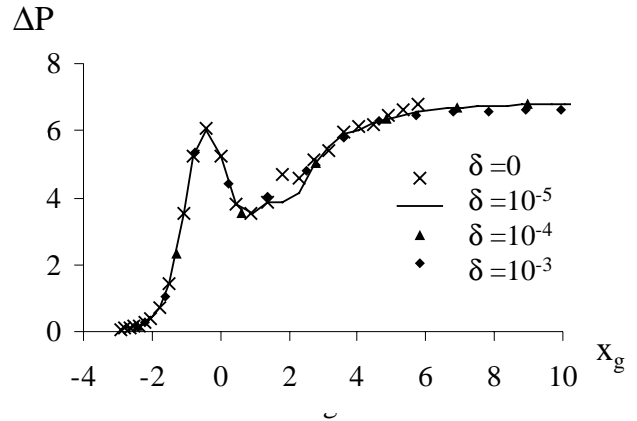


Figure 3 : Pressure drop variation for different values of the bending ratio δ ($A=B=0.8$, $\epsilon=0.12$, $\lambda=1$, NH membrane).

the exact value of v_g is not known, only the quantity $|v_r^M|$ can be studied to evaluate the precision of the proposed numerical scheme. Another global indicator of the precision of the numerical model is given by the final volume variation between the initial ($V_{ini} = \frac{4}{3}\pi AB^2$) and steady deformed shapes, which should be zero in principle.

Spatial convergence of the numerical method was verified for $\epsilon=0.09$, $A=B=0.8$ and a NH membrane by means of mesh refinement using a time step $\Delta t=2.5 \times 10^{-4}$, low enough to ensure stability for all considered meshes (Table 1). Increasing the number of elements on C_M from 60 to 112 and from 112 to 224 shows that the numerical error on the value of $|v_r^M|$ is smaller than $O(\Delta\zeta)$. Furthermore, the volume variation varies approximately linearly with $\Delta\zeta$. In all cases presented throughout, the volume variation was less than 0.1% of the capsule initial volume. It can then be considered that the overall precision of the numerical results is $O(\Delta\zeta)$. Moreover, increasing the number of elements from 60 to 224 leads to a change in the steady pressure drop smaller than 0.18% (Table 1). Consequently, $N_M=60$ is chosen as the standard number of elements except in the case of very large deformations where it was found necessary (on the basis of the volume change) to increase the number of points (see for example section 4.4).

Since the steady equilibrium in the cylindrical part of the pore is independent on the entrance phase, the numerical results can be compared as a first validation with those obtained in I for an initially spherical capsule with a NH membrane, $\lambda=1$ and $\alpha=45^\circ$. In I, a finite difference

N_M	$\Delta\zeta$	x_g	$ v_r^M _{\max}$	$(V-V_{ini})/V_{ini}(\%)$	ΔP^{ss}
60	0.0523599	11.7255558	0.0000100	-0.0887481	7.1959
112	0.0280499	11.7254507	0.0000078	-0.0345955	7.1845
224	0.0140249	11.72542403	0.0000077	-0.0172439	7.1835

Table 1 : Influence of spatial discretization at steady state on the capsule center of mass position, the maximum of the absolute value of the radial velocity, the relative variation of volume and the steady pressure drop (NH membrane, $\delta=10^{-5}$, $A=B=0.8$, $\lambda=1$, $\epsilon=0.09$, $N_B=180$, $N_P=30$, $\Delta t=2.5 \times 10^{-4}$ and $V_{ini} = \frac{4}{3}\pi AB^2$).

method (with 113 collocation points) is used in conjunction with smoothing and volume correction (the two procedures were found necessary to ensure numerical stability). The steady profiles are compared for $\epsilon=0.12$ (corresponding to the value $\epsilon=0.04$ in I where ϵ is based on the membrane Young modulus rather than on the shear modulus). A very good agreement is obtained (Figure 4). It should be noted that only 60 boundary elements have been necessary in the present model to obtain the same degree of accuracy as in I.

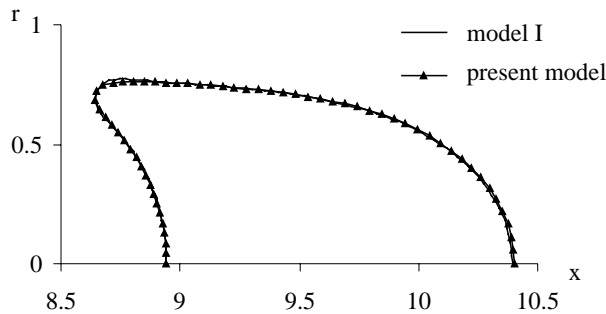


Figure 4 : Comparison of the steady profiles obtained here ($N_M = 60$) and in I ($N_M = 112$). Case: $A=B=0.8$, $\epsilon=0.12$, $\lambda=1$, NH membrane.

The absence of effect of λ on the steady state is verified for capsules with a SK membrane ($C=0$) and $\epsilon = 0.04$, for which a significant deformation is achieved. Steady deformed profiles are compared for different viscosity ratios ($\lambda=0.2; 1; 5; 10$) and for $x_g=11.84$. For initially spherical capsules, the steady profiles are superimposed within graphical precision (Figure 5a). For $\lambda=0.2; 1; 5$, the maximum values of $|v_x^M - v_g|$ and $|v_r^M|$ are of order 2.1×10^{-5} (Table 2), thereby indicating that steady state has been reached quite reasonably. Accordingly, the same steady values ΔP^{ss} are obtained for ΔP and for v_g within $O(\Delta\zeta)$, (i.e. at most 0.5%). For $\lambda=10$, owing to the

high internal viscosity, steady state has not been reached with the same precision. The maximum of $|v_x^M - v_g|$, although small, is about 50 times greater than for $\lambda=1$ or 5. The pressure drop is about 2% lower than for $\lambda=1$. This shows that very viscous capsules need a long length of tube to reach a steady state.

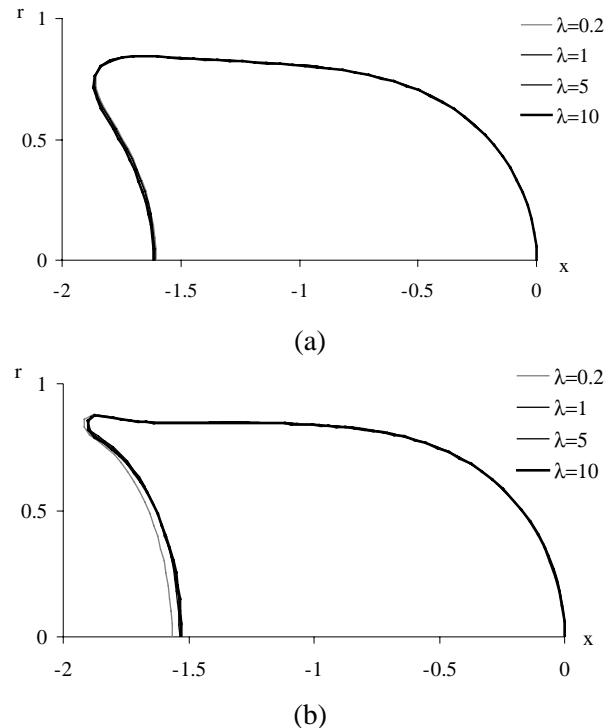


Figure 5 : Steady profiles of capsules for different values of λ ($R_{eq}=0.9$, $\epsilon=0.04$, SK membrane with $C=0$). a) initially spherical capsule $A/B=1$. b) ellipsoidal capsule $A/B=0.28$ $N_M=90$.

Similar results are obtained for initially ellipsoidal capsules (Figure 5b and Table 3). The same steady values are obtained for ΔP and for v_g within at most 1%. The maximum values of $|v_x^M - v_g|$ and of $|v_r^M|$ are now of order 2×10^{-3} . Furthermore, oscillations of ΔP (relative amplitude 0.05) are observed. They are probably due to the

numerical errors generated by the computations of the large curvatures that appear on the profile. In the micro-circulation of blood, it is well known that the red blood cells take on parachute shapes similar to the one shown on Figure 5b.

λ	v_g	ΔP^{ss}	$ \mathbf{v}_x^M - \mathbf{v}_g _{\max}$	$ \mathbf{v}_r^M _{\max}$
0.2	1.2048	14.3144	0.000018	0.000018
1	1.2047	14.3212	0.000017	0.000014
5	1.2053	14.2518	0.000019	0.000021
10	1.2076	14.0064	0.00095	0.000873

Table 2 : Center of mass velocity, steady pressure drop and relative velocity for different values of λ at position $x_g=11.84$. Initially spherical capsules : $A/B=1$, $R_{eq}=0.9$, $\varepsilon=0.04$, SK membrane with $C=0$ (Results obtained for 60 boundary elements).

λ	v_g	$\Delta P^{ss} (\pm 0.05)$	$ \mathbf{v}_x^M - \mathbf{v}_g _{\max}$	$ \mathbf{v}_r^M _{\max}$
0.2	1.1689	18.49	0.0021	0.0016
1	1.1717	18.30	0.0023	0.0020
5	1.1722	18.31	0.0018	0.0018
10	1.1734	18.20	0.0017	0.0013

Table 3 : Center of mass velocity, steady pressure drop and relative velocity for different values of λ at position $x_g=11.84$. Initially ellipsoidal capsules : $A/B=0.28$, $R_{eq}=0.9$, $\varepsilon=0.04$, SK membrane with $C=0$.

4.3 Effect of λ on the entrance process of capsules with different initial shapes.

We have shown that the viscosity ratio affects only the entrance phase into the pore. The entrance of capsules with NH or SK membranes has been studied for capsules with $\lambda=1$ (Leyrat-Maurin & Barthès-Biesel, I). The aim of this section is to appraise the effect of the viscosity ratio λ on the entrance phase of capsules with different sizes and shapes. The following results have been obtained for a SK membrane with $C=0$ and for $\varepsilon=0.04$.

4.3.1 Effect of size for a spherical capsule

The successive profiles of an initially spherical capsule ($R_{eq}=0.9$) as it enters the pore are shown on Figure 6a. The capsule first elongates and then takes an equilibrium parachute shape. The additional pressure drop ΔP first

increases to a peak value just before the entrance of the pore where partial plugging occurs (Figure 7a). It then decreases as the capsule takes an elongated shape to enter the pore. Although it creates a lower pressure perturbation, this elongated shape is not in equilibrium with the hydrodynamic forces, so that ΔP increases again to the equilibrium value that corresponds to the parachute profile. The effect of λ on ΔP or on v_g is weak (Figure 7a and b). However, the relaxation to steady equilibrium is longer for more viscous capsules: Figure 8 shows the profiles at time $t=18.7$ of two capsules with $A=B=0.9$, $\lambda = x$ and $\lambda=10$. The capsule ($\lambda=1$) has almost reached its steady state whereas the capsule ($\lambda=10$) has not.

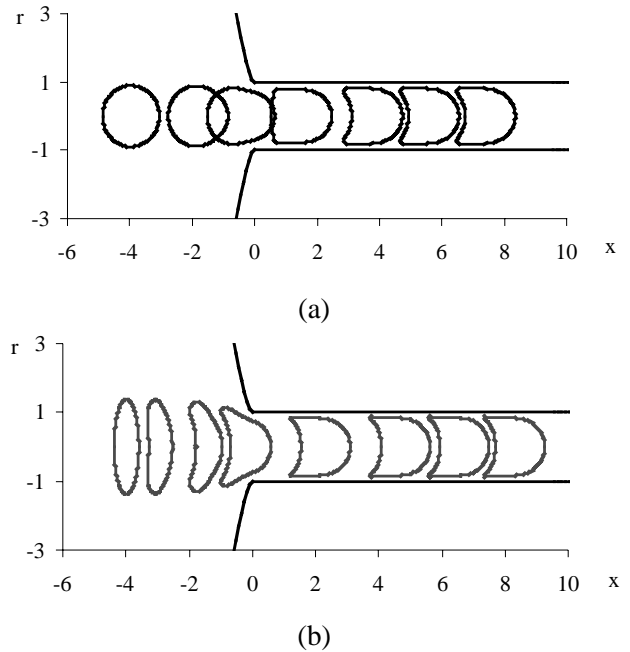


Figure 6 : Entrance of two isovolumic capsules ($R_{eq}=0.9$, SK membrane with $C=0$, $\varepsilon=0.04$). a) sphere $A=B=0.9$, b) ellipsoid $A/B=0.28$.

For large capsules ($R_{eq}=1.1$), the effect of λ on the entry peak of ΔP is enhanced because of the situation of quasi-plugging as the capsule enters the pore. Figure 9 compares the evolution of ΔP for initially spherical capsules with volumes corresponding to $R_{eq}=0.8$; 0.9, 1.1 and for $\lambda=1$ to 10. The volume plays an important role on the tube length (or time) necessary to reach a steady state, and on the steady value of pressure drop ΔP^{ss} . Indeed, an increase of 35% in capsule volume (from $R_{eq}=0.8$ to $R_{eq}=0.9$) leads to an increase of 48% in ΔP^{ss} .

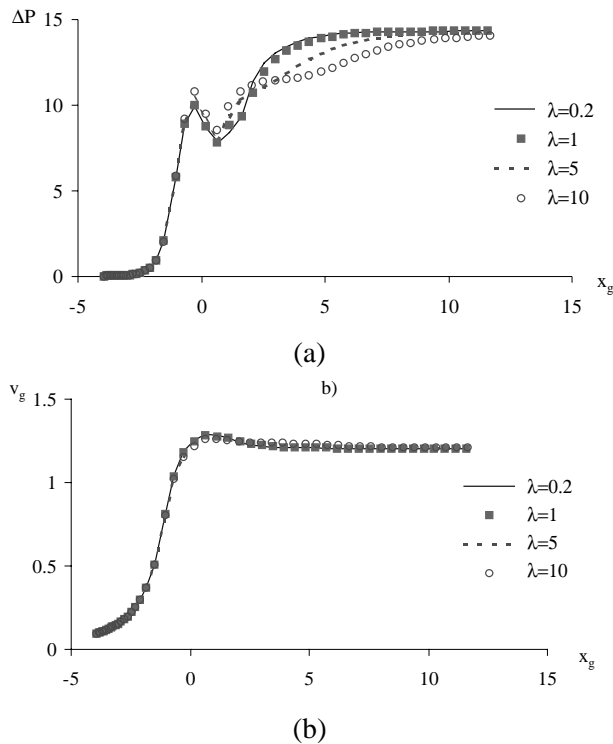


Figure 7 : Evolution of pressure drop ΔP (a) and of center of mass velocity v_g (b) with capsule center of mass position x_g for different values of the viscosity ratio λ ($A=B=0.9$, SK membrane with $C=0$, $\epsilon=0.04$).

4.3.2 Effect of capsule geometry

The capsule initial shape is also an important parameter. The successive profiles of an ellipsoidal capsule ($A/B=0.28$, $R_{eq}=0.9$) are shown on Figure 6b. As compared to a spherical capsule with the same volume, the ellipsoidal capsule behaves differently. During the entrance phase, the capsule ($A/B=0.28$) almost plugs the pore. The entry peak of pressure drop is thus larger and more λ dependent than for a spherical capsule (Figure 10). Owing to its excess surface area, as compared to the isovolumic spherical capsule, the ellipsoidal capsule creates a 26% larger steady pressure drop (Tables 2 & 3). However, the steady center of mass velocity is only slightly smaller for the ellipsoidal capsule (Tables 2 & 3). This indicates that volume is the main parameter that determines v_g , whereas ΔP^{ss} depends on both volume and geometry. However, the entrance time is longer for an ellipsoidal capsule than for a spherical one, as can be seen on Figure 11 which shows the time evolution of the center of mass position for the two capsules with $\lambda=5$.

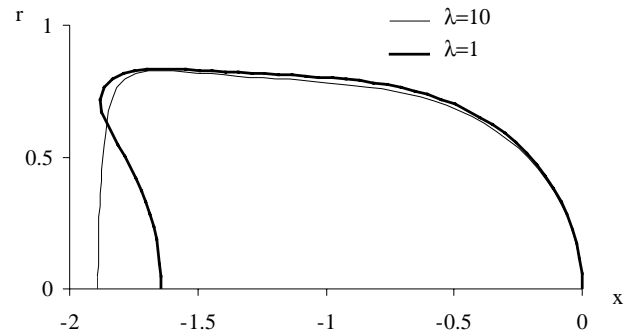


Figure 8 : Profiles obtained at time $t=18.7$ for two capsules with $\lambda = 1$ ($x_g=3.46$) and $\lambda=10$ ($x_g=3.44$). $A=B=0.9$, SK membrane with $C=0$, $\epsilon=0.04$.

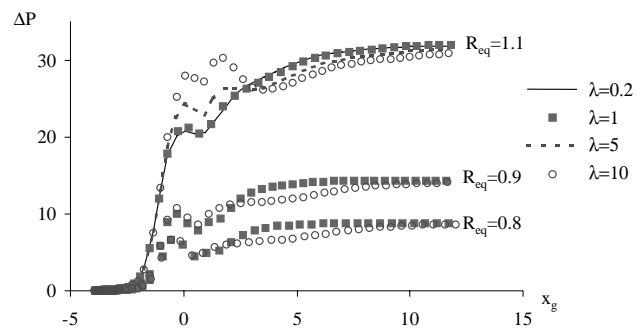


Figure 9 : Pressure drop for initially spherical capsules with different volumes ($R_{eq}=0.8$; 0.9 ; 1.1) and for different values of λ (SK membrane with $C=0$, $\epsilon=0.04$).

4.4 Effect of membrane constitutive law

In order to study the effect of the membrane constitutive law, we compare identical capsules (same initial geometry, same small deformation behavior), but with different membrane rheology (NH or SK), flowing under the same flow conditions (same ϵ and $\lambda = 1$). We first focus on a small enough value of ϵ ($\epsilon=0.09$) for which a steady state exists.

The steady deformed profiles of two spherical capsules ($R_{eq}=0.9$) are shown on Figure 12. The NH capsule is more deformed than the SK capsule. The steady additional pressure drop is slightly smaller for the NH capsule ($\Delta P^{ss}=11.12$) than for the SK one ($\Delta P^{ss}=12$) (Figure 13). This may be due to the fact that the liquid film surrounding the NH capsule is slightly thicker than the one around the SK capsule as shown on Figure 14. The front tips of the two capsules are very similar although the local meridian extensions are 22% different (Figure 15).

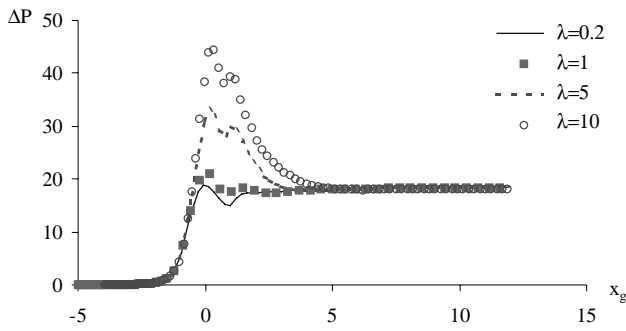


Figure 10 : Effect of λ on the pressure drop for an initially ellipsoidal capsule ($A/B=0.28$, $R_{eq}=0.9$, SK membrane with $C=0$, $\epsilon=0.04$, $N_M=90$).

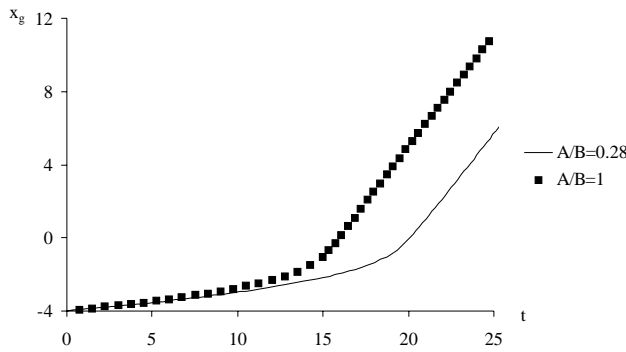


Figure 11 : Time evolution of the position of the center of mass of two isovolumic capsules with two different aspect ratios ($R_{eq}=0.9$, SK membrane with $C=0$, $\epsilon=0.04$, $N_M=90$ for $A/B=0.28$).

For initially ellipsoidal capsules ($A/B=0.28$), the effect of membrane law on the steady shape is important (Figure 16). The high curvature at the rear of the NH capsule leads to numerical errors and the variation of volume is thus of 0.1% at steady state for $N_M=112$. However, the NH capsule is considered to have reached equilibrium, since the maximum values of $|v_x^M - v_g|$ and $|v_r^M|$ are of order 5×10^{-3} . The SK capsule is less deformed with a maximum value of λ_s of 1.26. Correspondingly, the volume variation is smaller (0.075%) than in the NH case. The effect of membrane law and capsule geometry on steady deformation is summarized in Figure 17. The local meridian extensions of a NH capsule, either spherical or ellipsoidal, are shown on Figure 17a. The extension ratio is larger in the case of an ellipsoidal capsule, particularly at the downstream tip where the local extension is 23% larger for the ellipsoid than for the sphere ($\lambda_s = 1.40$ for $A/B=1$ and $\lambda_s = 1.72$ for $A/B=0.28$). For a

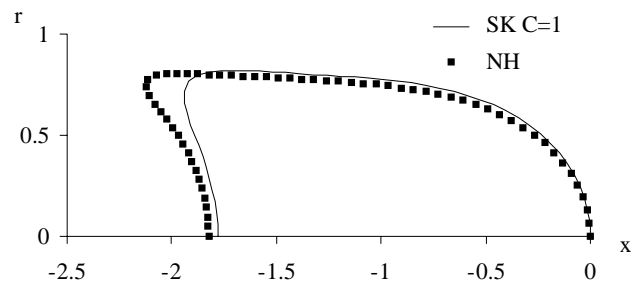


Figure 12 : Steady profiles of two initially spherical capsules with a NH or SK membrane ($A=B=0.9$, $\lambda=1$, $\epsilon=0.09$).

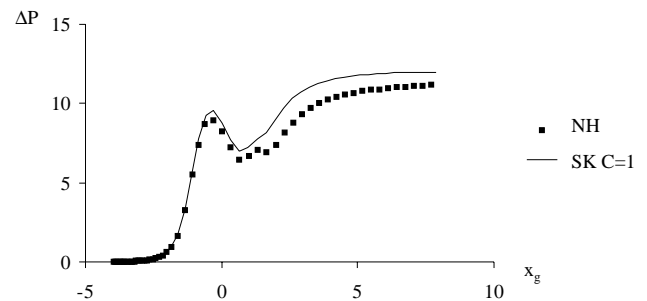


Figure 13 : Pressure drop variation of two initially spherical capsules with a NH or SK membrane ($A=B=0.9$, $\lambda=1$, $\epsilon=0.09$).

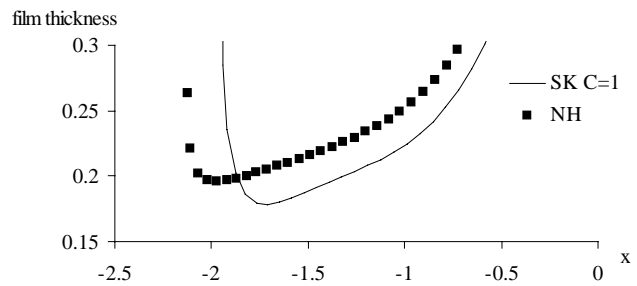


Figure 14 : Detail of the film thickness of two initially spherical capsules with a NH or SK membrane ($A=B=0.9$, $\lambda=1$, $\epsilon=0.09$).

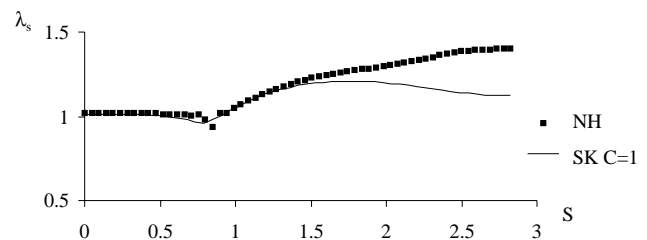


Figure 15 : Steady meridional extension ratio λ_s distribution versus initial arc length S for two initially spherical capsules with a NH or SK membrane ($A=B=0.9$, $\lambda=1$, $\epsilon=0.09$).

SK capsule, the strain hardening effect of the law leads to a weaker difference in local deformation between the spherical and ellipsoidal cases (Figure 17b).

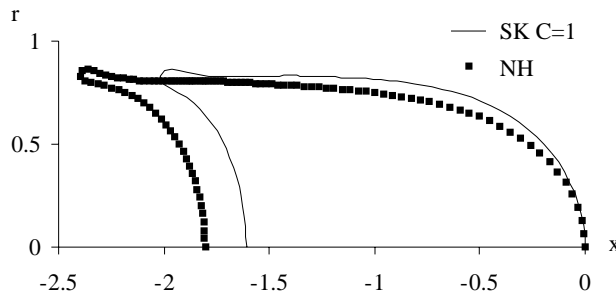


Figure 16 : Steady profiles of two ellipsoidal capsules with a NH or SK membrane ($A/B=0.28$, $R_{eq}=0.9$, $\lambda=1$, $\varepsilon=0.09$, $N_M=112$ for NH, $N_M=90$ for SK).

It is interesting to note that, for an ellipsoidal capsule, the steady pressure drop does not depend significantly on the membrane rheology (Figure 18), although there are some oscillations of ΔP^{ss} for both the SK (amplitude 0.1) and the NH cases (amplitude 0.15). The amplitude of the oscillations is larger than that observed for an ellipsoidal capsule with an SK membrane. $C=1$ and $\varepsilon = 0.04$ (section 4.3). This is probably due to numerical errors in the curvature computation. Surprisingly enough, the entry pressure peak is larger for the NH capsule (presumably more deformable) than for the SK one. The SK material is less amenable to deformation than the NH one under equivalent stress. This limits the deformation of the SK capsule and thus creates a smaller transient plugging effect. A similar effect is probably observed for a red blood cell, which has a SK membrane with $C \gg 1$.

Burst occurs because some break-up criterion (based on either deformation or stress) for the membrane material has been exceeded. Such break-up criterion is not included in the present model. If it were, membrane burst could be easily predicted since the local deformations and tensions in the membrane are computed. There is however a specific process that leads ineluctably to the burst of the capsule. Indeed it has been observed [Li, Barthes-Biesel and Helmy (1988); Diaz, Pelekasis and Barthes-Biesel (2000), I] that in some cases, when the capillary number exceeds a critical value ε_c , there is no possible equilibrium between the elastic and the viscous stresses. The capsule then elongates continuously until of course burst occurs. It is this mode of burst that

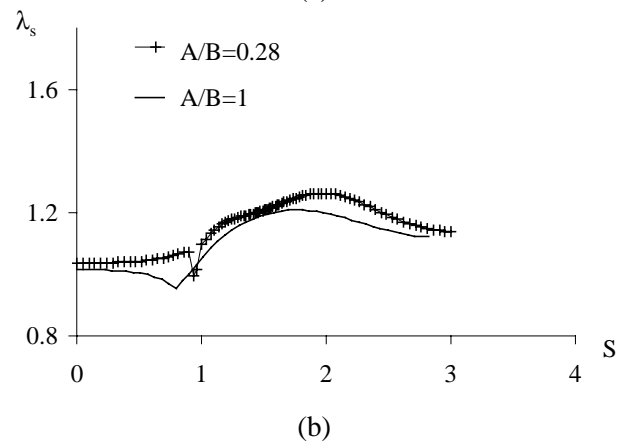
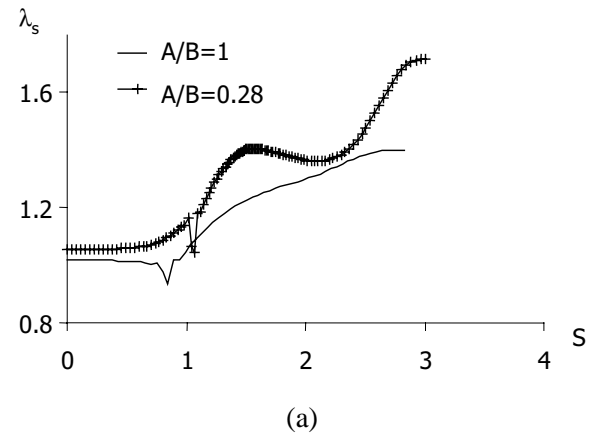


Figure 17 : Distribution of steady meridional extension ratio λ_s for two isovolumic capsules ($R_{eq}=0.9$, $\lambda=1$, $\varepsilon=0.09$), a) NH membrane $N_M=112$, b) SK membrane $N_M=90$.

we consider now. Consequently, we set ε to a large value ($\varepsilon = 0.18$) and simply monitor the maximum value of the meridian extension ratio $(\lambda_s)_{max}$ as a function of x_g for two spherical ($A=B=0.9$) capsules with NH and SK membranes (Figure 19). The maximum extension ratio $(\lambda_s)_{max}$ of a SK capsule reaches a equilibrium plateau value, indicating that the capsule SK reaches a steady state. This may be attributed to the strain-hardening behavior of the SK material. For the NH capsule however, $(\lambda_s)_{max}$ grows continuously, as had been observed before (I). Using two different spatial partitions ($N_M=50$ and $N_M=100$) leads to the same conclusion for the NH capsule.

5 Conclusion

The entrance of a capsule in a pore may be sensitive to the capsule initial shape, volume and internal viscosity.

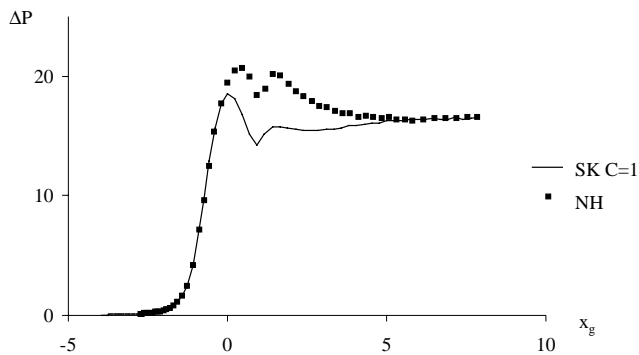


Figure 18 : Pressure drop variation of two initially ellipsoidal capsules with a NH or SK membrane ($A/B=0.28$, $R_{eq}=0.9$, $\lambda=1$, $\epsilon=0.09$, $N_M=112$ for NH, $N_M=90$ for SK).

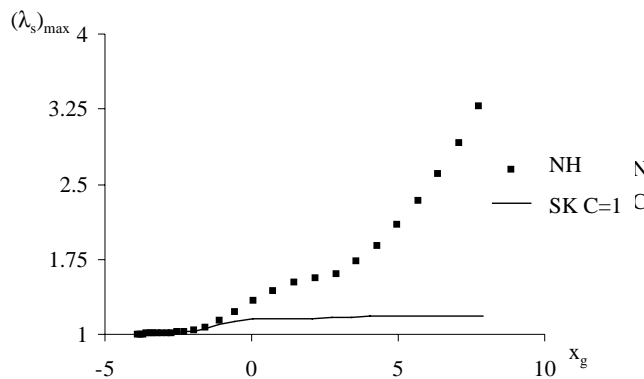


Figure 19 : Evolution of maximum meridional extension ratio $(\lambda_s)_{\max}$ with center of mass position x_g for a capsule with a NH membrane and a capsule with a SK membrane ($A=B=0.9$, $\lambda=1$, $\epsilon=0.18$).

The introduction of some bending rigidity of the membrane allows to study elongated ellipsoidal capsules. The effect of λ is weak as long as a situation of quasi-pore plugging has not been reached. Area compressible membranes with different large deformation behavior have been compared. Membrane rheology is an important parameter only in the regime of large deformations. The existence of a critical capillary number past which no steady state exists has been confirmed for a capsule with a neo-Hookean membrane. No such critical value has been found for capsules with a Skalak type, strain hardening, membrane. The model may provide information for the analysis of several experimental configurations such as the cell transit analyzer experiments. In this these experiments, a very dilute suspension of red blood cells

flows through a micropore filter. The change in electric resistance of the filter as one cell passes through one pore is monitored [Fisher, Wenby and Meiselman (1992)]. In the present model, the occupied pore electrical resistance may be readily estimated supposing the Maxwell approximation for long conductor [Deblois and Bean (1970)]. Moreover, the present model, which allows to relate the capsules deformed profiles to the membrane rheology, could be used to characterize the mechanical behavior of bioartificial capsules. The interesting characteristic of this flow configuration is that during the entrance process, the capsule is subjected to transient hydrodynamics stresses involving simultaneously area dilatation and simple shear. It would then be interesting to compare the numerical predictions with corresponding experimental results.

Finally, the model could easily be extended to treat the case of a train of capsules in a tube. In particular, it would be interesting to consider the case of two capsules which are close enough for hydrodynamic interactions to modify the single capsule solution as regards the additional pressure drop created by each particle.

References

- Barthès-Biesel, D. ; Diaz, A., Dhenin, E.** (2002) : Constitutive laws for two dimensional membranes : effects on capsule motion in flow", *J. Fluid Mech.* **vol 460**, 211-222
- Barthès-Biesel, D. ; Rallison, J.** (1981) : The time independent deformation of a capsule freely suspended in a linear flow. *J. Fluid Mech.*, **vol 113**, 251-267.
- Barthès-Biesel, D. ; Sgaier, H.** (1985) : Role of membrane viscosity in the orientation and deformation of a spherical capsule suspended in shear flow. *J. Fluid Mech.*, **vol 160**, 119-135.
- Brunn, P.** (1983): The deformation of a viscous particle surrounded by an elastic shell in a general time-dependent linear flow-field. *J. Fluid Mech.*, **vol 126**, 533-544.
- Couillette, C. ; Pozrikidis, C.** (1998) : Motion of an array of drops through a cylindrical tube. *J. Fluid Mech.*, **vol 358**, 1-28.
- Dagan, Z.; Weinbaum, S.; Pfeffer, R.** (1982): An infinite-series solution for the creeping motion through an orifice of finite length. *J. Fluid Mech.*, **vol 115**, 505-523.

- Deblois, R.; Bean, C.** (1970) : Counting and sizing of submicrons particles by the resistive pulse technique. *Rev. Sci. Inst.*, **vol 41** (7), 909-916.
- DeBoor C.** (1978) : A practical guide to Splines, Springer, New York.
- Diaz, A.; Pelekasis, N.; Barthès-Biesel, D.** (2000) : Transient response of a capsule subjected to varying flow conditions : effect of internal fluid viscosity and membrane elasticity. *Phys. Fluids*, **vol 12**, 948-957.
- Diaz, A.; Barthès-Biesel, D.; Pelekasis, N.** (2001) : Effect of membrane viscosity on the dynamic response of an axisymmetric capsule, *Phys. Fluids*, **vol 13**, 3835-3838.
- Fisher T.C.; Wenby R.B.; Meiselman H.J.** (1992): Pulse shape analysis of RBC micropore flow via new software for the cell transit analyser (CTA). *Biorheology*, **vol 29**, 185.
- Green, A. ; Adkins, J.** (1970) : Large elastic deformations. *Clarendon Press*, Oxford.
- Green, A. ; Zerna W.** (1968) : Theoretical elasticity. *Clarendon Press*, Oxford.
- Kwak, S. ; Pozrikidis, C.,** (2001) : Effect of flexural stiffness on the deformation of capsules in uniaxial extensional flow, *Phys. Fluids*, **vol 13** (5), 1234-1242.
- Kühtreiber, W.; Lanza, R.; Chick, W.**(1999) : Cell encapsulation Technology and Therapeutics, *Birkhäuser, Boston*.
- Lévy, M.C.; Edwards-Lévy, F.** (1996): Coating alginate beads with cross-linked biopolymers: a novel method based on a transacylation reaction, *J. Microencapsulation*, **vol 13**, 169-183.
- Le Tallec, P.; Mouro, J.** (2001) : Fluid structure interaction with large structural displacements , *Comput. Methods Appl. Mech. Engrg*, Volume 190 (24-25), 3039-3067
- Leyrat-Maurin, A. ; Barthès-Biesel, D.** (1994) : Motion of a deformable capsule through an hyperbolic constriction. *J. Fluid Mech.*, **vol 279**, 135-163.
- Li, X.; Barthès-Biesel, D. ; Helmy, A.** (1988) : Large deformation and burst of a capsule suspended in an elongational flow. *J. Fluid Mech.*, **vol 187** 179-196.
- Lim, F.** (1984): Biomedical applications of microencapsulation. *CRC Press, Boca Raton, Florida*
- Lipowski, R.** (1991) : The conformation of membranes, *Nature*, **vol 349**, 475-481.
- Martinez, M. ; Udell, K.** (1990) : Axisymmetric creeping motion of drops through circular tubes. *J. Fluid Mech.*, **vol 210**, 565-591.
- Pozrikidis, C.** (1990a) : The axisymmetric deformation of a red blood cell in uniaxial straining Stokes flow. *J. Fluid Mech.*, **vol 216**, 231-254.
- Pozrikidis, C.** (1990b) : The instability of a moving viscous drop. *J. Fluid Mech.*, **vol 210**, 1-21.
- Pozrikidis, C.** (1992) : Boundary integral and singularity method for linearized viscous flow, *Cambridge University Press, Cambridge*.
- Pozrikidis, C.** (1995) : Finite deformation of liquid capsules enclosed by elastic membranes in simple shear flow. *J. Fluid Mech.*, **vol 297**, 123-152.
- Pozrikidis, C.** (2001) : Effect of membrane bending stiffness on the deformation of capsules in simple shear flow *J. Fluid Mech.*, **vol 440**, 269-291.
- Quéguiner, C. ; Barthès-Biesel, D.** (1997): Axisymmetric motion of capsules through cylindrical channels.” *J. Fluid Mech.*, **vol 348**, 349-376.
- Rallison, J. ; Acrivos, A.** (1978) : A numerical study of the deformation and burst of a viscous drop in an extensional flow. *J. Fluid Mech.*, **vol 89**, 191-200.
- Ramanujan, S. ; Pozrikidis, C.** (1998) : Deformation of liquid capsules enclosed by elastic membrane in simple shear flow: large deformation and effect of fluids viscosities. *J. Fluid Mech.*, **vol 361**, 117-143.
- Reid, H.; Barnes, A.; Lock, P.; Dormandy, J.** (1976) : A simple method for measuring erythrocyte deformability. *J. Clin. Pathol.*, **vol 29**(9), 855-858.
- Secomb, T. ; Hsu, R.** (1996) : Analysis of red blood cell motion through cylindrical micropore : effect of cell properties. *Biophys. J.*, **vol 71**, 1095-1101.
- Skalak, R.; Tözeren, A.; Zarda, P.; Chien; S.** (1973) : Strain energy fonction of red blood cell membranes. *Biophys. J.*, **vol 13**, 245-264.
- Stone, H.; Leal, L.** (1989) : Relaxation and breakup of an initially extended drop in an otherwise quiescent fluid. *J. Fluid Mech.*, **vol 198**, 399-427.
- Stroud, A.; Secrest, D.** (1966) :“Gaussian quadrature formulas”. *Prentice-Hall, EngleCliffs, NJ*.
- Youngren, G.; Acrivos, A.** (1976) : On the shape of a gas bubble in a viscous extensional flow, *J. Fluid Mech.*, **vol 76**, 433-442.

Zarda, P.; Chien, S.; Skalak, R. (1977): Elastic deformations of red blood cells. *J. Biomech.*, **vol 10**, 211-221.

Zhou, H. ; Pozrikidis, C. (1995) : Deformation of liquid capsules with incompressible interfaces in simple shear flow. *J. Fluid Mech.*, **vol 283**, 175-200.

